Journal of Structural Geology, Vol. 14, No. 7, pp. 857 to 871, 1992
Printed in Great Britain

0191-8141/92 $05.00+0.00
Pergamon Press Ltd

Analysis of tilting near normal faults using calculus of variations: implications for upper crustal stress and rheology

ROB WESTAWAY

Department of Geological Sciences, University of Durham, South Road, Durham DH1 3LE, U.K.

(*Received* 3 *July* 1991; *accepted in revised form* 1 *April* 1992)

Abstract—An initially-horizontal surface in the surroundings to a normal fault will, after extension, tilt towards the fault if in the hanging-wall or away from it if in the footwall. Coseismic deformation of these surroundings can be validly modelled as flexure. Cumulative deformation on geological time scales has been regarded as flexure also, but this has led to the apparent paradox that many observed structures require the effective elastic thickness of the brittle upper crust to be much smaller than its seismogenic thickness. This article presents a possible alternative: that cumulative deformation of the upper crust near some active normal faults may be regarded instead as partitioned into separation of the blocks that comprise their surroundings (through the horizontal component of dip-slip on the fault) and distributed vertical simple shear in their surroundings, which causes them to tilt and takes up the vertical slip on the fault. A generalized profile of tilting near a normal fault, which approximates a parabola, can be derived following two assumptions. First, the brittle layer retains an elastic term in its rheology on geological time scales, such that it resists arbitrary length changes. Second, the brittle layer minimizes its overall vertical deflection, thus minimizing the buoyancy force acting on it. Maximum stress and total strain energy associated with observed profiles of tilting are typically smaller for distributed vertical simple shear, favouring this mechanism over flexure.

INTRODUCTION

DURING deformation of the continental lithosphere, extension of the brittle upper crust is typically taken up on sets of normal faults with subparallel strike and a common slip vector (e.g. Westaway 1991). As extension proceeds, normal faults typically develop less steep dip, and beds in the hanging-wall of any normal fault will generally tilt towards it. Where faults are spaced by $\leq$20 km (comparable to the $\leq$15 km thickness of the brittle layer), blocks between them typically take up extension by tilting uniformly in a manner that is sometimes likened to rigid-body rotation of 'dominoes' around horizontal axes (e.g. Jackson 1987). Other regions contain more widely-spaced normal faults, up to ~100 km apart (e.g. Westaway 1991), between which blocks do not tilt uniformly. Instead, the parts of each block that are within ~15 km of any major fault become deflected—tilting progressively towards that fault if in its hanging-wall or away from it if in its footwall—and the remaining parts remain undeformed.

Extension of the brittle layer in many such regions is taken up by slip on normal faults of these types, and appears to be largely, perhaps entirely, coseismic. Effort has thus been devoted to studying the physics of the coseismic deformation, which occurs in a few seconds during large earthquakes, and understanding how it develops into long-term deformation, both on interseismic time scales of hundreds or thousands of years and on geological time scales of millions of years. Many normal faults are approximately planar throughout the brittle layer (e.g. Stein & Barrientos 1985, Jackson 1987). Coseismic elevation change has been regarded as an effect of flexure, and has been modelled as deformation around a finite planar cut in an elastic halfspace (e.g. Savage & Hastie 1966, Mansinha & Smylie 1971). This is valid, because even on the ~1 year time scale often required to survey 'coseismic' deformation, the rheology of the crust and upper-mantle lithosphere is dominated by their elastic properties. The resulting equations for elastic deformation of the surroundings to a normal fault mean that coseismic elevation change at any point at the Earth's surface depends on the coseismic slip at all points on the fault. Although these equations thus enable observed elevation change profiles to be numerically modelled in terms of coseismic slip distributions, they do not reveal analytically the expected shape of these profiles.

As a result of the requirements for isostatic equilibrium, absolute coseismic hanging-wall subsidence on any isolated normal fault is expected (e.g. Savage & Hastie 1966, 1969, Jackson & McKenzie 1983) and observed (e.g. Stein & Barrientos 1985) to be 5–10 times greater than absolute footwall uplift. In contrast, on longer time scales the lower crust will deform plastically, which will modify the form of profiles of tilting away from what is expected for the coseismic case (e.g. King *et al.* 1988). The principal observable effect on interseismic time scales is absolute uplift of both the footwall and hanging-wall (e.g. Koseluk & Bishke 1981, King *et al.* 1988), which over each complete earthquake cycle increases absolute footwall uplift and decreases absolute hanging-wall subsidence relative to the coseismic values, such that they may become roughly equal. This process appears to be driven to some extent by flow from the flanks into the lower crust beneath each normal fault, and to some extent by flow from beneath the hanging-wall to beneath the footwall (e.g. King *et al.* 1988). This doming has been observed following some large normal-faulting earthquakes, such as Fairview Peak and Hebgen

Lake in the western U.S.A. (Koseluk & Bishke 1981, Reilinger 1986). Some people (e.g. Wernicke 1985, Weissel & Karner 1989) have suggested that active normal faults may persist to the base of the continental lithosphere. If so, such doming would not be expected (see e.g. Koseluk & Bishke 1981) and profiles of tilting would have much greater width than is typically observed. In contrast, it seems preferable to adopt the view that normal faults die out at the base of the brittle upper crust into the plastic deformation of the underlying lithosphere. The observation that coseismic and long-term deformation typically have the same ~15 km width requires low 'effective elastic thickness' of the upper crust if the long-term deformation is modelled as flexure (e.g. King *et al.* 1988).

Although long-term footwall uplift and hanging-wall subsidence are expected to be roughly equal in the absence of erosion or loading, loading of the hanging-wall with either water or sediment will usually make it subside farther than the distance by which the footwall uplifts. The overall relative size of hanging-wall subsidence and footwall uplift on geological time scales across any real active normal fault will thus depend on many factors, such as the extents of footwall erosion and of sedimentation in hanging-walls and any other topographic lows around the fault, and the sediment density. These will depend on other factors such as the local rock types, average elevation of the Earth's surface and climate. Because these vary with each fault, recent work on the evolution of active normal faults on geological time scales has, like for coseismic deformation, mainly involved numerical modelling rather than exploring analytic solutions for idealized cases.

King *et al.* (1988) seem to be the first people to have published numerical solutions that involve realistic physics on the coseismic, interseismic and geological time scales, for the problem of coupling the elastic deformation around active normal faults in the brittle layer to the underlying plastic deformation. Their method determines a full solution for the vertical deflection of the Earth's surface, with a limited number of free parameters for rheology of the crust and displacement on each fault. However, their long-term rheology did not simply comprise an elastic upper crust over a fluid lower crust. Instead, the upper crust comprised a lower elastic layer overlain by an upper layer that behaved differently, being assumed instead to transmit load and vertical deflection to the underlying elastic layer. Buck (1988) and Weissel & Karner (1989) have independently presented similar numerical solutions. Some approximations are involved in these numerical methods, the validity of which is addressed, for example, by Buck (1988). King & Ellis (1990) have developed another numerical method, which involves specifying the stress at all points on each fault, but which allows all three components of the resulting displacement to be determined.

Others (e.g. Kusznir & Egan 1990, Marsden *et al.* 1990, Kusznir *et al.* 1991) have established a simpler numerical approach, the flexural cantilever method, which involves assuming values for additional parameters that are not directly observable, such as the width of plastic deformation in the lower crust. They treat the upper crust as elastic but allow for the possibility that localized brittle failure in the surroundings of any normal fault may modify bending stress relative to that expected for an unbroken elastic layer.

The different numerical methods make some different predictions that are potentially observable. For example, Kusznir *et al.* (1991) predict that, in the absence of sediment loading or erosion, long-term footwall uplift and hanging-wall subsidence are equal provided the flow in the lower crust is symmetrical about the fault zone. King *et al.* (1988) predict more complex behaviour, where their ratio depends on fault dip and, to a small extent, on the density contrast between the lower and upper crust. With 45° fault dip and no density contrast, they also predict equal footwall uplift and hanging-wall subsidence.

If all or part of the brittle layer deforms by flexure on geological time scales, any vertical deflection of the surroundings to a normal fault will be accompanied by horizontal displacement that is associated with contraction or dilation near the top or base of the brittle layer (e.g. King & Ellis 1990, Kusznir *et al.* 1991) (Fig. 1). King & Ellis (1990) suggested that this process may cause elastic strains of the order of ~0.07 in the brittle layer. However, other studies indicate that crustal rock typically fails in tension at strain $\leqslant 10^{-4}$. This upper limit on elastic dilational strain follows since the tensile strength of unbroken rock is typically ~10 MPa (e.g. Kusznir *et al.* 1991) and its Young's modulus is ~100 GPa. Kusznir *et al.* (1991) suggested also that once maximum bending stress in the surroundings to a normal fault exceeds ~1 GPa (which, during flexure, will occur at bending strain $\geqslant 10^{-2}$, given Young's modulus ~100 GPa), brittle failure will relieve this high stress. Brittle failure may be most important in hanging-walls where

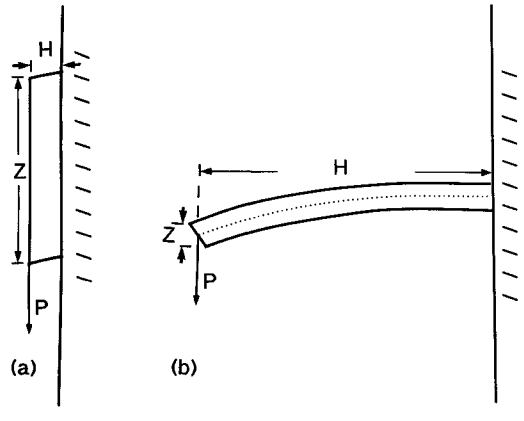

Fig. 1. Comparison of distributed vertical simple shear and flexure for localized loads applied to initially horizontal beams that are embedded in a rigid support at one end. If the aspect ratio (Z/H) of the beam is large, it will accommodate loading by distributed vertical simple shear, as in (a). If this ratio is small, the beam will accommodate loading by flexure, as in (b). Note that in both cases the upper and lower faces of the beam develop curved profiles. In (a) the free end of the beam remains vertical, whilst in (b) it acquires a slope. In (b) the upper part of the beam dilates and the lower part shortens.

bending stress causes dilation at shallow depth, making tensional failure most likely. Whether this creates a single antithetic normal fault or results in pervasive fracturing, it will lead to the brittle layer evolving differently than if it had not occurred. With the brittle layer ~10 km thick and elastic bending strain limited to $\leq 10^{-2}$, elastic bending displacements (relative to the local equilibrium position in the absence of bending strain) cannot exceed ~50 m. They are thus small compared with typical throws and heaves on major normal faults, which may reach many kilometres.

Active normal faults typically occupy the uppermost ~10–15 km of the continental crust, which deforms brittlely and is thus expected to have elastic thickness ~10–15 km. However, many studies have established that structures that form following the development of substantial heave on normal faults often require much smaller 'effective elastic thickness': frequently ~3–4 km, sometimes <1 km (e.g. Buck 1988, Stein *et al.* 1988, King & Ellis 1990). This contrasts with other effects, such as deflection of oceanic lithosphere near subduction zones and surface loads, which can be modelled flexurally with values of parameters that are known independently to be reasonable, and which show features such as peripheral bulges that are unequivocally caused by flexure.

Flexure of an elastic layer depends on its flexural rigidity, which is proportional to its Young's modulus and the cube of its thickness; it does not depend on these parameters individually. Reducing 'effective' elastic thickness from ~10–15 km to ~3 km is thus equivalent to reducing Young's modulus by a factor of ~100, from ~100 to ~1 GPa. The low flexural rigidity or 'effective elastic thickness' required to match observed long-term deformation may thus be caused by a small Young's modulus, not a small elastic thickness. King & Ellis (1990) scaled Young's modulus by this factor throughout the brittle layer. King *et al.* (1988) reduced effective elastic thickness by assuming instead that only the lower part of the brittle layer remains elastic on geological time scales. Both these views consequently predict low 'effective elastic thickness' on geological time scales regardless of the heave on any particular fault. In contrast, Kusznir *et al.*'s (1991) suggestion, that the observed low 'effective elastic thickness' on geological time scales follows brittle failure at the high bending stress that would otherwise accompany the development of ≥1 km of heave, would predict that the surroundings to normal faults with smaller heave would show 'effective elastic thickness' of the brittle layer comparable to its seismogenic thickness. Buck (1988) also suggested that 'effective elastic thickness' decreases with increasing heave for similar reasons, but its value may depend on the curvature of the brittle layer in each locality rather than being uniform. Substantial differences thus exist between these views and, although 'effective elastic thickness' is a familiar term, its physical meaning has not previously been resolved.

If the shallow part of the hanging wall dilates as a result of flexure, and the deeper part contracts, there will be a particular depth z_0—the depth of the neutral fibre—where length is unchanged. In the footwall, the shallow part will contract and the deeper part will dilate under flexure. If w is the vertical deflection, and $w'' = d^2w/dx^2$, where x is horizontal position (Fig. 2a), elastic bending strain ε_{xx} at depth z is:

$$\varepsilon_{xx}(x, z) = (z_0 - z)w''(x). \quad (1)$$

The corresponding bending stress σ_{xx} is:

$$\sigma_{xx} = \frac{\varepsilon_{xx}E}{1 - \nu^2}, \quad (2)$$

where E is Young's modulus and ν is Poisson's ratio. The thin plate approximation usually used to analyse flexure, which leads to these equations, assumes that vertical stress σ_{zz} is zero and shear stress σ_{xz} is negligible compared with σ_{xx}. E and shear modulus μ are related as $E = 2\mu(1 + \nu)$: with $\mu = 30$ GPa and $\nu = 0.25$, E is 75 GPa; with $\mu = 40$ GPa, E is 100 GPa. If sustained by flexure in a 10 km thick brittle layer ($|z_0 - z|$ up to ~5 km) with $E = 75$ GPa, the substantial maximum curvature w'' of the brittle layer (which, as is shown later, reaches ≥0.03 km^{-1} near most normal faults considered) would require bending strain up to ~0.1 and bending stress up to ~10 GPa. Even if the maximum value of $|z_0 - z|$ where deformation remains elastic with this Young's modulus were ≤1 km, maximum values of σ_{xx} would still be ≥1 GPa. The sharpness of observed curvature of profiles of tilting near normal faults thus also requires small 'effective elastic thickness' if it is modelled flexurally (see also, for example, Buck 1988). Even allowing for brittle failure in some parts of the brittle layer, elastic bending stress must still reach many hundreds of MPa if the observed curvature arises by flexure (Kusznir *et al.* 1991).

The rheology of the brittle layer evidently retains an elastic term on geological time scales: it would otherwise be unable to support topography. For a difference in surface elevation h of adjacent localities in rock with density ρ, the vertical stress σ_{zz} at depth will be $\sim\rho\mathbf{g}h$, where $\mathbf{g}$ is the acceleration of gravity. With $\rho \sim 3000$ kg m^{-3}, the typical maximum ~4 km topography near many normal faults (e.g. Westaway 1991) (between the top of the basement in the footwall and hanging-wall) causes local *vertical* stress ≤120 MPa: roughly 10 times smaller than the maximum *bending* stress predicted assuming flexure with the parameters listed above. Once this scale of topography has formed, many normal fault zones develop further with additional en échelon branches (e.g. Westaway 1991), enabling extension to continue without adding to the topography, rather than by increasing the throw on existing faults. Anderson's theory of fault mechanics predicts *horizontal* stress is also no greater than ~100 MPa in a ~10 km thick brittle layer (see, for example, Turcotte & Schubert 1982, p. 355). These observations suggest that near normal faults the brittle layer may only support stresses ≤100 MPa on long time scales, and the larger bending stresses required for flexure are thus difficult to explain.

In other localities, such as Death Valley in California (King & Ellis 1990), larger displacements develop on individual active normal fault branches, with sharper curvature in their surroundings. This may be feasible because the lower crust is relatively hot and weak, with relatively low viscosity (e.g. Buck 1988). In these cases erosion of the uplifting footwall may limit the topography across the fault and hence the vertical stress. Some people (e.g. Buck 1988, King & Ellis 1990) have suggested that after extreme extension such structures may develop into metamorphic core complexes, but the precise physical processes responsible have been widely debated. Other normal faults develop comparable heave and deflection in their surroundings, but these surroundings show very gentle curvature, with tilting distributed over much greater width. The Mesozoic Jeanne d'Arc basin offshore of Newfoundland is a good example (see Kusznir *et al.* 1991).

Blocks beside any normal fault may thus undergo local dilation or contraction, with elastic bending strain never greater than ~0.01. The horizontal displacements associated with this bending will be small compared with the heave on many normal faults, which may reach many kilometres. Near a normal fault that has taken up kilometres of extension, one can thus to a good approximation neglect relative horizontal displacements that result from such bending, and regard the amount of extension across the fault as equal to its heave. If horizontal displacements other than the heave itself are neglected entirely, displacements of points on each side of a normal fault will be vertical only. Such deflection varying with horizontal position is equivalent to distributed vertical simple shear.

Following this assumption, the length (in the direction perpendicular to a fault) of profiles of tilting will increase at all depths within the brittle layer, rather than remaining constant (as would occur if the brittle layer were infinitely rigid) or dilating or contracting above and below a neutral fibre (as would occur under flexure), but the amount of upper crustal mass within each element with horizontal extent dx will remain constant (Figs. 1 and 2a). Although some length changes in the brittle layer are thus inevitable if it takes up vertical shear, its finite elastic strength on geological time scales will oppose arbitrary length changes. The question thus arises: should tilting on either side of a normal fault on geological time scales be regarded as flexure that mimics vertical shear because horizontal displacements are small? Or (as suggested, for example, by Wernicke & Axen 1988) is it better to regard it instead simply as vertical shear?

ANALYTIC SOLUTIONS FOR TILTING NEAR NORMAL FAULTS

Buoyancy forces caused by topography will influence the form of profiles of tilting of the Earth's surface or any other initially-horizontal surface near any normal fault. If sediment loading and erosion are neglected, the Moho is assumed flat (such that buoyancy forces caused by any Moho topography are neglected), and crustal density ρ is assumed uniform, the vertical buoyancy force per unit area of the Earth's surface f_b will equal the weight of crust displaced:

$$f_b = \rho g w, \tag{3}$$

where $w(x)$ is the vertical deflection and $\mathbf{g}$ is the acceleration of gravity. This force will be upward beneath the hanging-wall and downward beneath the footwall. The buoyancy force dF_b (per unit along-strike length) acting between horizontal positions x and $x + dx$ will equal $f_b dx$ (Fig. 2a):

$$dF_b = \rho g w dx. \tag{4}$$

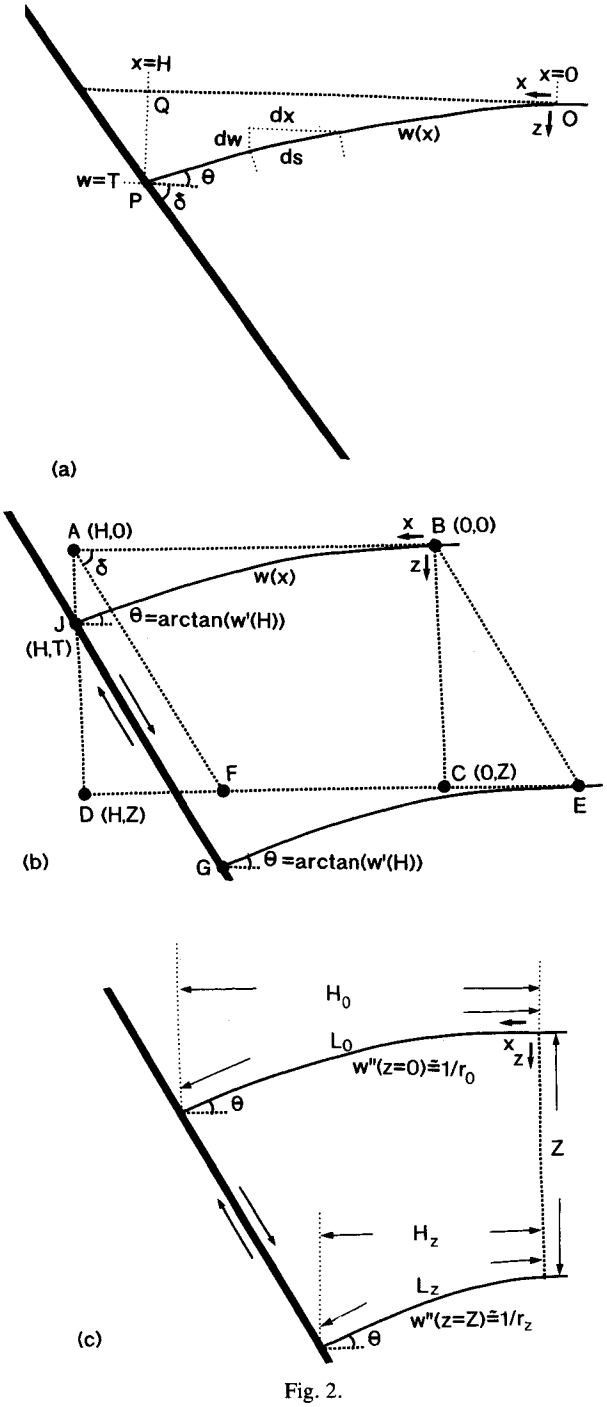

Fig. 2.

The buoyancy force between $x = 0$, where displacement reaches zero, and $x = H$, is thus:

$$F_b \int_0^H \rho g w dx. \quad (5)$$

However, if minimizing buoyancy forces were the only constraint, it would be attainable with $w(H) = T$ and $w(x < H) = 0$ (i.e. with w varying as a step at the fault) and $F_b = 0$. This would conflict with the substantial width of deflection observed near real normal faults.

Given that the rheology of the brittle layer includes an elastic term on geological time scales, let us assume that within it an elastic restoring force acts, which is proportional to the length change of a profile across it (i.e. proportional to length OP–OQ in Fig. 2a). If the brittle layer tilts by distributed vertical simple shear, any element of it with initial length dx will develop final length $ds = (1 + w'^2)^{1/2}$, where $w' = dw/dx$. The elastic restoring force will thus be proportional to $\int ds - dx$ (Fig. 2a).

In principle, one could solve the equation of equilibrium for each element of the brittle layer to obtain the deflection profile $w(x)$ for which no resultant force acts. This is what is usually done to obtain flexural solutions, given the approximations and assumptions already noted (see, for example, Turcotte & Schubert 1982, pp. 112–119, Ranalli 1987, pp. 203–210). However, it is difficult to do more generally, for reasons discussed, for example, by Buck (1988). The approach followed here instead looks for solutions that minimize the buoyancy force acting on the brittle layer subject to the constraint on its length. This leads to an idealized profile of tilting, which is shown to match observations reasonable well and is sufficiently general to explore the different deformation styles that may cause such profiles. The form of the brittle layer is thus assumed to be governed by the need to minimize total buoyancy force $F_b = \int \rho g w dx$ subject to the constraint that profile length after deformation $L = \int ds$ equals the appropriate final value. This can be achieved by considering the integral:

$$I' = \int_0^H (\rho g w + k(1 + w'^2)^{1/2})\, dx, \quad (6)$$

where k is a Lagrange multiplier. This equation can be simplified by dividing through by k and substituting $j = \rho g/k$ to give

$$I = \int_0^H (jw + (1 + w'^2)^{1/2})\, dx = \int_0^H f(w, w')\, dx, \quad (7)$$

where j is another Lagrange multiplier, with dimensions of reciprocal length. One first finds the minimum of this integral with j undetermined, then finds the value of j that gives the appropriate length. As will become clear, minimizing any function of this form (where $w(x)$ and $w'(x)$ are constrained to reach zero at the same value of x) gives a profile that is approximately parabolic.

The application of calculus of variations to derive the profile of tilting that minimizes the integral in equation (7) is contained in Appendix A. The resulting profile is:

$$w = r(1 - (1 - x^2/r^2)^{1/2}), \quad (8)$$

where

$$r = \frac{H^2 + T^2}{2T} \simeq \frac{H^2}{2T}, \quad (9)$$

where H is the horizontal extent of the deflection and T is the maximum deflection (at $x = H$). Equation (8) can usually be well approximated as:

$$w = x^2/2r \quad (10)$$

because r is usually much greater than H, the upper limit of x. Having established this general form of profiles of tilting, other parameters can be derived from it.

The final length L of a profile between $x = 0$ and $x = H$ will be

$$L = \int_{x=0}^{x=H} ds. \quad (11)$$

Using the exact form for $w(x)$ (equation 8),

$$L = r \arcsin\left(\frac{H}{r}\right). \quad (12)$$

Using instead the approximate form (equation 10),

$$L = H\left(1 + \frac{H^2}{6r^2}\right). \quad (13)$$

Using the approximate form for $w(x)$, total buoyancy force F_b (from equation 5) is:

Fig. 2. Schematic diagram showing the co-ordinate system used to describe profiles of tilting near normal faults, illustrated for a hanging-wall. Co-ordinates x and z denote horizontal and vertical position, measured from an origin where deflection $w(x)$ reaches zero. w increases from zero at $x = 0$ to T at $x = H$. In a reference frame fixed relative to the origin, the point now at P was originally at Q, and the length of the profile has thus increased from the straight line OQ = H to the arc length OP = L. dx is an element of length in the x-direction, and ds is an element of arc length along the profile. From Pythagoras' theorem, $ds^2 = dx^2 + dw^2$. Thus $ds = dx(1 + w'^2)^{1/2}$, where $w'(x) = dw/dx$. (b) Schematic diagram comparing dimensions of regions used for integration to obtain elastic strain energy with dimensions of the tilting near real normal faults. Integration is carried out over the rectangle ABCD with width H and height Z. For distributed vertical simple shear w in this rectangle is independent of depth. It represents the complex shape BEGJ that indicates the likely true extent of deflection in basement in the brittle layer (assuming vertical shear), where the arc length BJ (or EG) equals L. This shape has the same area as the parallelogram ABEF that has the same area as ABCD. In reality, for the fault to remain planar with dip δ, tilt θ must be the same at all depths beside it. The integration thus mimics the assumption that tilt at a given distance from the fault is the same, regardless of depth, by making tilt the same (regardless of depth) at a given distance from the edges AD and BC. (c) An alternative possibility that is not pursued here. Tilt is assumed uniform beside the fault, but the width of deflection varies with depth, with w reaching zero at all depths beneath the same horizontal position ($x = 0$). This requires w'' to increase with depth, making r decrease with depth (given equation A18). Uniform tilting at the fault requires $H(z)/r(z)$ to be the same at all depths (equation A17), requiring $r \propto H$. From equation (13) $L(z)/H(z)$ is thus the same at each depth (i.e. $L_z/H_z = L_0/H_0$), indicating average dilation is the same at each depth. This scheme can thus represent a more complex form of distributed vertical simple shear.

Table 1. Some well-documented normal faults

Name	T (km)	H (km)	r (km)	Z (km)	H/r	r/Z	σ_{xx}^{max} (MPa)	σ_{xy}^{max} (MPa)	E_l (MPa)
Draugen (F) (a)	1.5	10	33	≤15	0.30	>2.2/ 2.8	162	121	990
Draugen (F) (b)	1.5	16	85	≤15	0.19	>5.7/ 2.8	162	194	4080
Troll (F)	0.2	7.5	70	≤15	0.11	>4.7/ 8.6	76	43	1580
Denizli (H)	0.4	6	45	~10	0.13	4.5/ 7.3	95	53	1010
Cricket Mtn (F)	1.6	10	32	~15	0.31	2.1/ 2.7	250	125	640
Grand Valley (F) (a)	0.6	7	40	~15	0.18	2.7/ 5.0	200	70	560
Grand Valley (F) (b)	0.6	9	160	~15	0.07	10.7/16.5	50	31	3520
Lost River (F)	1.6	15	70	<20	0.21	>3.5/ 4.0	107	86	2250
Death Valley (F)	≥7	10	10.6	~10	0.95	1.1/ 2.6	580	308	320
Jeanne d'Arc (H)	14	110	430	~10	0.26	40 / 3.0	~12	~100	142,000

F and H after fault names denote footwall and hanging-wall. T, H and r are throw, width of tilting and radius of curvature (r being estimated using equation 17). E_l is the long-term Young's modulus estimate from equation (17). Z is the brittle layer thickness, either known from seismicity (Lost River) or from the spacing of main and antithetic faults (Denizli, Grand Valley) or inferred (others). In the column r/Z the observed value is followed by the limiting value for flexure. If this limiting value is larger, distributed simple shear is favoured. σ_{xx}^{max} and σ_{xy}^{max} are the maximum stresses assuming flexure and distributed vertical simple shear, calculated for $x = H$ and $z_0 = Z/2$ assuming Young's modulus 1 GPa (equivalent to shear modulus 0.4 GPa with Poisson's ratio 0.25). The Draugen and Troll faults (late Jurassic) are in the North Sea: see Roberts & Yielding (1991) (their fig. 3 shows locations and figs. 6 and 8 show cross-sections). The Denizli fault (upper Miocene–Pliocene to present) is in western Turkey: see Westaway & Kusznir (in press). The Cricket Mountain and Grand Valley faults are described in the text. The Lost River fault (Miocene to present) is mentioned in the text (it slipped in the Borah Peak earthquake); see Stein *et al.* (1988) (their figs. 4 and 5 show its location and a cross-section). The Death Valley fault in SE California was discussed by King & Ellis (1990) (their fig. 2 shows a cross-section). The Jeanne d'Arc basin is in the western North Atlantic: see Kusznir *et al.* (1991) (their fig. 13 shows a cross-section).

$$F_b = \frac{\rho g H^3}{6r}. \quad (14)$$

The Lagrange multiplier k, introduced in equation (6), satisfies

$$j = \rho g / k \quad (15)$$

or

$$k = \rho g r. \quad (16)$$

Suppose Z is the vertical extent of the change in profile length from H to L on geological time scales, and equals the vertical extent of the associated elastic stress. For vertical shear Z thus equals the brittle layer thickness. If E_l is an estimate for the long-term Young's modulus of the brittle layer (a measure of the ratio of its cumulative stress to cumulative strain), such that the elastic restoring force (per unit along-strike length) in the brittle layer equals $E_l(L - H)Z/H$, then from equation (6) k will equal $E_l Z/H$. Hence,

$$E_l = \frac{\rho g r H}{Z}. \quad (17)$$

With $\rho = 3000$ kg m^{-3} and $\mathbf{g} = 10$ m s^{-2}, r ~30 km (a typical lower limit established later), H ~10 km, and Z ~15 km, E_l is ~1 GPa. This is comparable to the values used by King *et al.* (1988), Stein *et al.* (1988) and King & Ellis (1990), and is ~1% of reasonable values for the short-term Young's modulus of crustal rock. Values of E_l vary by a factor of up to ~3 about this value (Table 1). Table 1 also includes estimates of maximum shear stress (assuming vertical shear) and bending stress (assuming flexure). For the same elastic moduli, vertical shear typically requires smaller maximum stress.

If the surroundings to a planar normal fault take up vertical shear on geological time scales, then a well-defined relationship exists between the tilt angles of the fault and of initially horizontal beds or other surfaces adjacent to it (Westaway & Kusznir 1990, in press). If δ_0, δ and θ denote initial and final fault dip and the tilt angle of a surface adjacent to the fault that was horizontal when extension began (Fig. 2), then:

$$\tan(\theta) = \tan(\delta_0) - \tan(\delta). \quad (18)$$

Initial dip δ_0 of any normal fault whose surroundings take up vertical shear can thus be estimated from δ and θ. Note that equation (18) typically predicts $\theta > \delta_0 - \delta$, and thus differs from the widely-used assumption of rigid-body rotation beside any normal fault, where θ equals $\delta_0 - \delta$. An initially-horizontal surface is thus expected to develop the same tilt on both sides of a fault provided the fault remains planar with uniform dip throughout the brittle layer. Numerical models based on flexure also typically predict that beds tilt more than adjacent faults (as is clear from careful inspection of figures in the various publications), although they do not satisfy equation (18) precisely.

This suggestion of distributed vertical simple shear in basement beside normal faults that tilt during extension, and the angular relationship that it predicts, differs in principle from the geometrical method of Verrall (1981)—the 'Chevron construction'—where an extensional basin is assumed to develop by distributed vertical simple shear in soft sediment that collapses onto the fixed rigid footwall of a fault that does not tilt during extension. This method has been modified to incorporate inclined simple shear (White *et al.* 1986), although retaining the assumption of a rigid footwall. In both forms it is thus unsuitable for investigating basins above planar faults that tilt and cut basement that is the same in

the footwall and hanging-wall (see also Kusznir *et al.* 1991).

OBSERVED PROFILES OF TILTING NEAR NORMAL FAULTS

In many localities, tilting of initially-horizontal surfaces may result from the effects of slip on many faults. The above analytic solutions cannot conveniently describe these regions, which are best investigated numerically instead. This section therefore covers isolated normal faults instead, addressing both cumulative and coseismic deformation.

Cumulative deformation across the Grand Valley fault zone, Idaho

The Grand Valley normal fault zone in the western U.S.A. (for location see, for example, Dixon 1978, or Anders *et al.* 1989) has present-day dip is ~55° at the Earth's surface, and is isolated, there being no other major normal fault within ≥25 km on either side. The surface of the hanging-wall sedimentary basin, at 1700 m, is 300 m below this regional level. This basin is bounded on the far side by a smaller antithetic fault (the Snake River fault), and shows a ~−10 mgal gravity anomaly (Mabey 1985) which can give the maximum sediment thickness provided the average density contrast is known. Westaway (1990) assumed -300 kg m^{-3} density contrast, which gives ~1000 m maximum thickness, similar to the value reported by Dixon (1978). The mountain range in its uplifted footwall rises to ~2400 m. If the profile of its topography is projected towards this fault to compensate for likely erosion since this fault became active, maximum elevation would be ~2500 m: ~500 m above the regional average. This reasoning indicates that throw across the Grand Valley fault is ~1800 m. Beyond this basin and the immediate vicinity of the fault in its footwall, the topography is used to indicate the profile of a surface that was roughly horizontal before this fault became active (Fig. 3).

Both the footwall and the hanging-wall, including its part between the two faults, can be matched using curves of the form of equation (8). Figure 3(a) has maximum tilt ~9° on both sides of the main fault. This equal tilting is consistent with precisely planar geometry; equation (18) gives initial dip ~58°. However, the different r values imply different E_1, and hence different rheology, which is unreasonable as the basement on both sides of this fault is the same (e.g. Dixon 1978). Figure 3(b) shows an alternative match, with r the same on both sides but with tilt slightly different. The excess of hanging-wall tilting is consistent with slight listric curvature of the fault at depth. Such curvature has been noted on some other normal faults that cut basement elsewhere (e.g. Westaway *et al.* 1989), and would not be unreasonable. The solution in Fig. 3(b) is thus preferable on these grounds.

Cumulative deformation across the Cricket Mountain fault, Utah

This ~40 km long normal fault segment, which has been studied by Stein *et al.* (1988) (see their fig. 6 for location), strikes SSW, dips WNW at ~52°, and has taken up Neogene extension. Cricket Mountain has formed along the central part of its uplifted footwall, with summit at 2150 m, 800 m above the surrounding basin. The southern part of the well-known Wasatch fault (e.g. Schwartz & Coppersmith 1984) has similar strike and passes ~50 km ESE of Cricket Mountain. No structure in between shows significant Neogene extension. Farther west, numerous faults that took up substantial early Tertiary extension show no evidence for significant Neogene activity. There is thus no other major active normal fault within ~50 km of the Cricket Mountain fault.

Stein *et al.* (1988) presented results of seismic reflection profiling along an E–W line that crosses this fault obliquely near its northern end, where both the footwall and hanging-wall are buried by young sediment. One reflector in the footwall, at depth 1.5 km when ≥10 km from the fault, is a 4.2 Ma old basalt flow. Stein *et al.* (1988) interpreted a similar reflector at similar depth

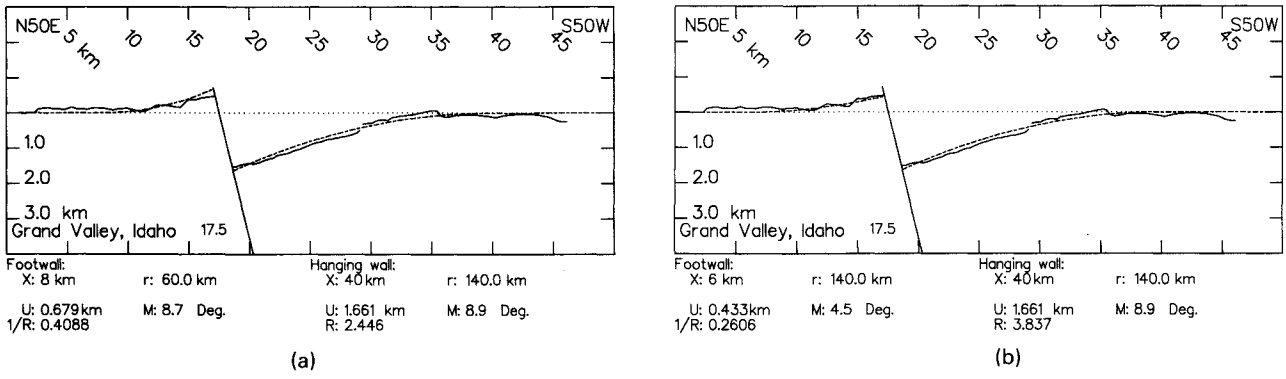

Fig. 3. Observed and predicted profiles of top basement for the Grand Valley profile of Westaway (1990). The Grand Valley fault is drawn schematically with 55° dip, and vertical distance is relative to the typical ~2000 m elevation when far from the fault. In this and subsequent figures: X is the horizontal position (measured perpendicular to fault strike) where predicted deflection reaches zero; U is the maximum deflection; M is the slope of the fitted curve at the fault; R is the predicted ratio of maximum footwall uplift to maximum hanging wall subsidence; and r is the radius of curvature. (a) Profiles assuming the same maximum tilt on both sides of the fault. (b) Profiles assuming the same curvature on both sides of the fault.

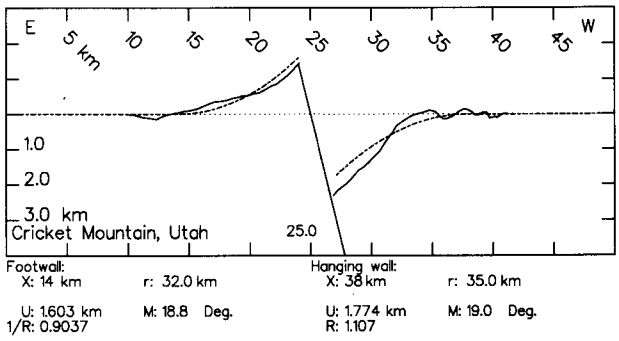

Fig. 4. Observed and predicted profiles of the reflector from the Cricket Mountain seismic reflection profile of Stein *et al.* (1988). The Cricket Mountain fault is drawn with 52° dip, and vertical distance is relative to the level of the reflector when distant from the fault. This is ~2000 m below the Earth's surface and thus ~600 m below sea level.

≥10 km inside the hanging-wall as the same flow. Figure 4 shows the profile of this interpreted unit (from their Fig. 8b) against distance along this profile. Their Fig. 8(c) indicates that reflections at 6–7 km inside the hanging wall are weak, and it is consequently difficult to be sure whether they have correctly extrapolated the same reflector between this point and the fault. If their interpretation is accepted, this fault has taken up ~5 km of slip since 4.2 Ma, at average rate ~1 mm year^{-1}, similar to rates on other nearby active normal faults, including the Wasatch fault (e.g. Schwartz & Coppersmith 1984). Given the fault dip, this slip has accompanied ~3 km of heave and ~4 km of throw since 4.2 Ma.

Figure 4 shows a fit to the reflector on both sides of the Cricket Mountain fault. The ~19° predicted maximum tilt indicates initial fault dip ~58°, given the ~52° present-day dip. Although this match accounts for observed tilts reasonably well, it underestimates depth of the reflector near the fault in its hanging-wall. Several factors may contribute to this mismatch. First, the flow causing the reflection may not have been flat initially. Second, compaction of sediment beneath this flow may have distorted it. Third, compaction of the relatively thick sediment above this part of the flow would raise local sediment density above that typical elsewhere, causing additional local loading relative to the ideal used to derive equation (8). This would cause greater hanging-wall subsidence and less footwall uplift than is predicted, in better agreement with what is observed. The match in Fig. 4 is comparable to that obtained using flexural modelling by Stein *et al.* (1988) (see their fig. 11). The principal mismatch features, the overestimation of observed subsidence over ~31–35 km, and the underestimation over ~27–31 km, are indeed common to both.

Coseismic deformation across the Lost River fault, Idaho

Coseismic elevation change profiles have been surveyed after several major normal-faulting earthquakes (surface-wave magnitude $M_s > 6.5$, seismic moment $M_0 > 10 \times 10^{18}$ Nm). These include: Fairview Peak, Nevada (16 December 1954, M_s 7.1, M_0 ~53 × 10^{18} Nm; Doser & Smith 1989), Hebgen Lake, Montana (18 August 1959, M_s 7.5, M_0 ~100 × 10^{18} Nm; Doser 1985) and Borah Peak, Idaho (28 October 1983, M_s 7.3, M_0 ~21 × 10^{18} Nm; Doser & Smith 1989) in the western U.S.A.; Campania–Basilicata (23 November 1980, M_s 6.9, M_0 ~26 × 10^{18} Nm; Westaway & Jackson 1987) in Italy; Corinth (24 February 1981, M_s 6.7, M_0 ~11 × 10^{18}Nm; Jackson *et al.* 1982) in Greece; and Edgecumbe (2 March 1987, M_s 6.6, M_0 ~10 × 10^{18} Nm; Anderson *et al.* 1990) in New Zealand.

Several factors make most of these data sets unsuitable for testing general theory for tectonic elevation change beside a single fault. These include complexity of en échelon faulting (at Hebgen Lake and Edgecumbe; Savage & Hastie 1966, Barrientos *et al.* 1987, Beanland *et al.* 1990), sparseness (at Corinth; Mariolakos & Stiros 1987), the presence of antithetic faulting (at Campania–Basilicata and Fairview Peak; Romney 1957, Pantosti & Velensise 1990), discrepancies between versions of the same data set (at Fairview Peak; Reil 1957, Slemmons 1957, Whitten 1957), and possible contributions from landsliding or other superficial processes (at Campania–Basilicata and Edgecumbe; Westaway 1987, Beanland *et al.* 1990). Comparison is thus restricted to Borah Peak only, for which the data set is of good quality and well-distributed across a single planar normal fault. Although these data seem unique at present, there is no reason to believe that any other isolated planar normal fault would not show a similar profile.

The Borah Peak earthquake ruptured the SE-striking Lost River fault in central Idaho (see e.g. Stein & Barrientos 1985 for location). The observations in Fig. 5 are based on a relevelled profile that crossed obliquely the principal seismogenic fault segment near its midpoint. Uplift of ~30 mm was observed far from the fault on both sides. Given that formal uncertainties in elevation change are ~2 mm, this appears significant. It was presumably caused by regional-scale processes that are not directly related to slip on this fault, and has therefore been subtracted from the profile in Fig. 5. This residual elevation change profile shows smooth decreases from maxima at the fault to zero ≤20 km from it.

These coseismic elevation changes can be matched using curves of the form of equation (8) (Fig. 5). The

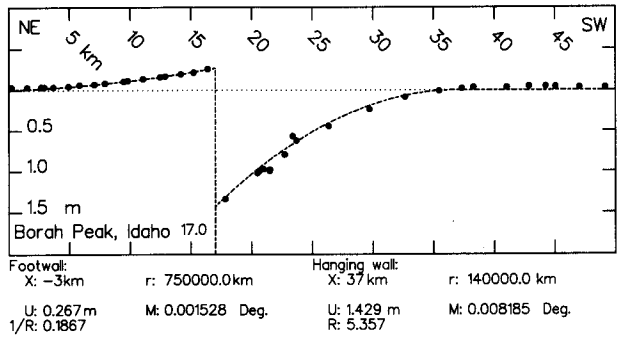

Fig. 5. Comparison of a predicted profile with coseismic elevation change observations by Stein & Barrientos (1985) for the Borah Peak earthquake.

match is comparable to the results of Stein & Barrientos (1985) and Barrientos *et al.* (1987) from elastic dislocation modelling, which gave 2.2 m typical slip and 49° fault dip. They thus estimated typical throw and heave as ~1.7 and 1.4 m. Aftershocks die out beyond ~12 km depth (e.g. Richins *et al.* 1987). The modelling by Barrientos *et al.* (1987) required the main fault to die out at ~14 km depth. In contrast, teleseismic waveform studies by Doser & Smith (1985) suggest centroid focal depth for the mainshock was 16 ± 4 km. The precise local thickness of the brittle layer is thus unclear. Assuming 16 km, with a neutral fibre at 8 km depth, with Young's modulus ~75 GPa, the $\sim 1.4 \times 10^{-6}$ km^{-1} hanging-wall curvature in Fig. 5 requires elastic bending stress up to ~4 MPa.

The coseismic tilting has similar width on both sides of the Lost River fault. The absolute coseismic displacement of the hanging-wall, which is ~5 times that of the footwall, requires larger r for the footwall than for the hanging-wall. Given equation (17), this appears to imply that the footwall is much stronger than the hanging-wall, which would make no sense as basement on both sides is the same (e.g. Stein & Barrientos 1985). The estimates of elastic moduli obtained using equation (17), ~30,000 GPa for the footwall and ~6000 GPa for the hanging-wall, are also unrealistic. It is not surprising that equation (17) gives unrealistic estimates in these circumstances, because for coseismic deformation elastic forces and displacements are not confined to the brittle layer, nor are they uniform within the brittle layer, as were assumed to derive this equation. As already noted, the observed coseismic ratio of footwall uplift to hanging-wall subsidence is explicable as the isostatic response to a finite cut in an elastic halfspace, and does not require different rheology on either side of the fault. Nonetheless, equation (8) gives a reasonable match to observations with a minimum of free parameters, and its prediction of bending stress is valid. Although the physics of coseismic and long-term deformation differ in detail (e.g. King *et al.* 1988), both depend to some extent on the interrelationship between elastic forces and buoyancy forces. Equation (8) appears sufficiently general to match both cases.

ELASTIC STRESS AND STRAIN ENERGY

This section investigates the elastic strain energy in the surroundings to normal faults, assuming that tilting follows equation (8). Fits of observed profiles to this equation indicate the significance of r, which is typically ~30 km for cumulative deformation near normal faults with T ~1 km, where values of x/r are typically $\leqslant 1/3$ (Table 1). Elastic strain energy is estimated in Appendix B for the alternative assumptions that any given profile of tilting, with radius of curvature r, width H and brittle layer thickness Z, arises either by flexure or by distributed vertical simple shear. Assuming flexure, strain energy is given by equation (B18) that can be approximated by equation (B20). Assuming instead vertical shear, strain energy is given by double equation (B5) that can be approximated by double equation (B8). Let W denote the ratio of elastic strain energy for flexure to that for vertical shear, with given values of r, H and Z. W can be evaluated exactly as the ratio of equation (B18) to double equation (B5). However, the resulting complex expression would then be difficult to interpret. If W is evaluated approximately instead as the ratio of equation (B20) to double equation (B8), it will not differ much from the exact estimate. Thus

$$W \simeq \frac{EZ^2}{4\mu(1-\nu^2)H^2} \tag{19}$$

or

$$W \simeq \frac{(1+\nu)Z^2}{2(1-\nu^2)H^2}. \tag{20}$$

For $W > 1$,

$$H < \frac{Z}{[2(1-\nu)]^{1/2}}. \tag{21}$$

If ν is ~0.25, for W to be >1, $H \leqslant 0.8\,Z$. If ν is 0.5, for W to be >1, $H \leqslant Z$.

The relative strain energies for the two deformation styles thus depend on the width of deformation H and the brittle layer thickness Z. One would expect the brittle layer to use the mechanism that minimizes its strain energy. For a given ratio H/r, strain energy for flexure is proportional to HZ^3, whereas strain energy for distributed simple shear is proportional to H^3Z. Decreasing H/Z keeping other parameters constant would decrease the energy for simple shear and increase the energy for flexure. Provided H/Z is small enough, more energy is required for flexure than for simple shear, and one would expect the deflection to be by vertical shear rather than by flexure, as in Fig. 1. Because Young's modulus and shear modulus are in proportion, this result is independent of their values.

Table 1 examines several normal faults given this reasoning. In the active examples, brittle layer thickness is known or inferred, and the observed width of deformation favours distributed vertical simple shear. For the late Jurassic examples from the North Sea, brittle layer thickness during extension is uncertain. However, it is unlikely to have been $\leqslant$10 km, which would be required for flexure to be favoured. Two values of H are listed for the Draugen fault, which provides a possible counterexample that would favour flexure if the larger alternative were adopted. The bed whose tilt profile gives this value (see fig. 6 of Roberts & Yielding 1991) is offset around ~10–15 km from this major fault by several minor faults, making it difficult to judge precisely where w reaches zero. The Lost River fault may provide another counterexample favouring flexure. A range of solutions exists for it, depending on the width of deformation H and brittle layer thickness Z. The range of H reflects uncertainty in the local structure, and other uncertainty discussed by Stein *et al.* (1988). The uncertainty in Z takes account of the different results discussed earlier. Some

Table 2. Parameters for normal faults associated with distributed vertical simple shear

Fault	μ (MPa)	σ_{xy}^{max} (MPa)
Draugen (a)	400	120
(Draugen (b))	1630	790)
Troll	630	70
Denizli	400	50
Cricket Mountain	260	80
(Grand Valley (a))	220	40)
Grand Valley (b)	1410	110
Lost River	900	190
Death Valley	130	100

Shear modulus μ is calculated from E_1 in Table 1 assuming Poisson's ratio 0.25. σ_{xy}^{max} is scaled from the value in Table 1 assuming the appropriate value of μ for each fault instead of the standard value of 400 MPa used in Table 1.

combinations favour vertical shear (Table 2); others favour flexure.

Because the approximate and exact estimates of strain energy differ minimally for $H/r \leq 1/3$, equation (21) may suffice to establish whether flexure is favoured even in some cases when curvature is substantial. However, where H/r is larger than ~1/3, as at Death Valley, the exact expressions must be used instead. Figure 6 shows the limiting value of r/Z for flexure as a function of H/r, assuming strain energy is given by equation (B18) for flexure and by double equation (B4) for vertical shear. Using values of H and T from King & Ellis (1990), the Death Valley footwall lies well inside the field where vertical shear is favoured.

DISCUSSION

The results of this study may be compared with earlier suggestions. They support the view of King *et al.* (1988), Stein *et al.* (1988) and King & Ellis (1990) that long-term deformation of the brittle layer can be modelled with Young's modulus typically ~1 GPa. Like these earlier studies, this study does not provide a physical explanation for why long-term Young's modulus is only ~1% of its short-term value. The smaller long-term Young's modulus dramatically reduces stress and strain energy density from the values that would arise if this parameter were larger. However, because shear modulus and Young's modulus are in proportion, this does not affect the ratio of strain energy for flexure and vertical shear.

As already noted, Kusznir *et al.* (1991) suggested that (for flexure) brittle failure when bending stress reaches ~0.5–1 GPa dramatically affects the subsequent evolution of the brittle layer. They suggested this effect becomes significant after a fault has taken up ≥1 km of heave, reducing maximum bending stress and causing 'effective elastic thickness' to decrease to only a few kilometres. However, several of the faults in Table 1 have throw (and hence heave, given dips ~45°) less than 1 km, but show similar values of parameters such as r, H and E_1 to other faults with larger heaves. Given that the hanging-wall curvature that developed in the Borah Peak earthquake required bending stress up to ~4 MPa, if such stress were to accumulate without interseismic relief, ~100 such earthquakes would create a situation approaching the failure conditions, but would account for only ~150 m of heave. Kusznir *et al.* (1991) may thus be correct that the evolution of normal faults changes dramatically once a heave threshold, determined by failure criteria, is exceeded, but this may be ~100 m, not ~1 km. The faults studied in this article thus all have too much heave to test this possibility. Faults with heave ≤100 m are indeed seldom studied in detail, effort usually being directed instead at larger structures that are considered more significant.

The critical respect in which the results of this study

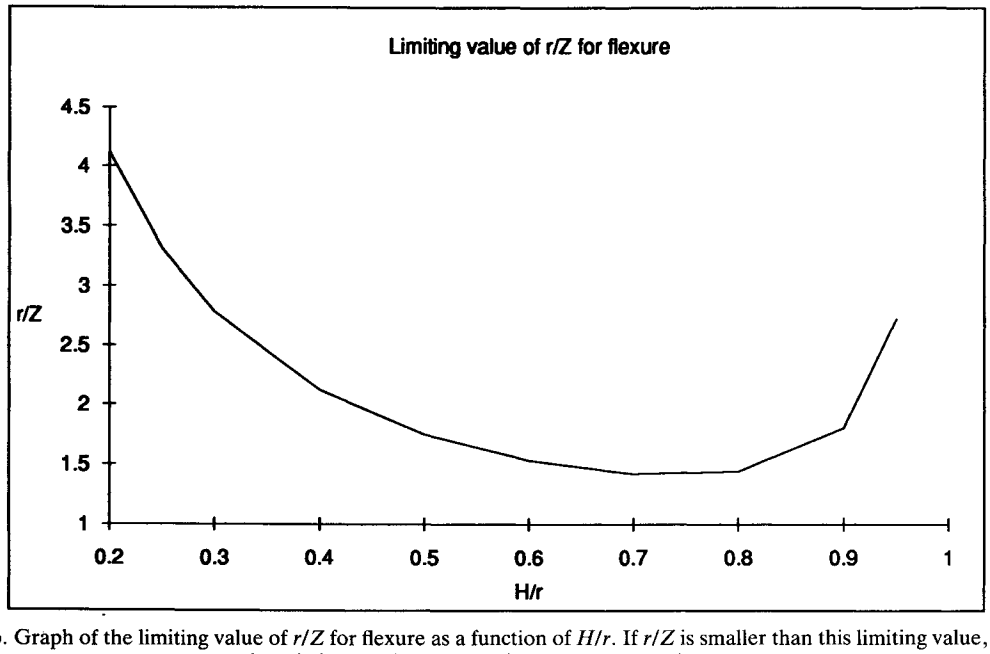

Fig. 6. Graph of the limiting value of r/Z for flexure as a function of H/r. If r/Z is smaller than this limiting value, vertical shear is favoured instead, as it requires less strain energy.

differ from earlier views is the suggestion that the principal deformation mechanism of the brittle layer around some normal faults with substantial heave is not flexure, but vertical shear. For the examples considered, this typically requires lower strain energy and maximum stress. If the brittle layer deforms by vertical shear, one would expect its deflection and tilt to decrease monotonically to zero, as in equation (8). Flexure allows for the possibility of a small peripheral hanging-wall bulge and/or footwall sag instead, and the demonstrable presence of either would thus be important in establishing that flexure occurs instead. However, no convincing example appears to have been documented.

The possibility of localized horizontal contraction in the concave-upward footwall 'knee' provides another potential criterion to distinguish flexure and vertical shear. The Earth's surface in the hanging-wall of any normal fault is expected to dilate under both flexure and vertical shear. However, in the footwall it is expected to contract under flexure but dilate under vertical shear. Thus the existence of folds in the footwall knee, with the same age as the adjacent normal faulting, would indicate contraction and thus confirm flexure. King & Ellis (1990) have claimed that such folds exist in footwalls of many normal faults in the western U.S.A., which have similar width of tilting to the structures considered in this article, and cite several examples. However, in some cases (e.g. for Death Valley and for the Virgin Mountain fault zone in northwestern Arizona) the age of the folds is unclear and may be greater than much or all of the normal faulting (see e.g. Axen & Wernicke 1989). In others, the observed folds are well dated but their tectonic setting is unclear. For example, folds reported by King & Ellis (1990) as documented by Gilbert & Reynolds (1973) in the footwall of the major E-dipping normal fault that bounds the eastern front of the Wassuk range in NW Nevada are, in fact, ~15 km from the fault, in the hanging-wall of another E-dipping normal fault a few kilometres farther west. Although these folds presumably have the same age as the adjacent normal faulting, they are thus not necessarily related to footwall flexure. As already noted, the Death Valley footwall has more likely developed by vertical shear than by flexure, and one would thus not expect contraction there anyway.

The results of this study suggest that a mechanism exists, which presumably operates on interseismic time scales, which converts coseismic deformation (which can be validly modelled as flexure) into long-term deformation (which appears instead to involve vertical shear). Others have suggested that pressure solution creep can be important within the upper crust on geological time scales (e.g. Turcotte & Schubert 1982, p. 335), and may provide the mechanism for reducing long-term Young's modulus, being driven by stress generated within the brittle layer by its coseismic response. The observation that the long-term coseismic deformation near any normal fault typically have the same width implies that this mechanism only operates in localities with coseismic displacement. If relaxation (converting coseismic flexure to vertical shear) proceeds by such a mechanism that occurs at non-zero values of local stress, it may proceed regardless of heave, and the surroundings to any normal fault may thus never approach the conditions for brittle failure.

If one accepts that long-term deformation near a normal fault is vertical shear, then three principal deductions follow. First, the heave equals the extension across the fault. The total extension across any cross-section containing many normal faults that cut the brittle layer will thus equal the sum of their heaves. Second, dip variations of faults and tilting of initially horizontal surfaces near them are related by equation (18). The usual assumption that tilting of blocks bounded by closely-spaced normal faults involves rigid-body rotation thus appears wrong in principle (see also Westaway & Kusznir in press). Third, it is shear stress, not bending stress, that determines the shape of profiles of tilting. Maximum shear stress appears comparable to the maxima of horizontal stress and vertical stress caused by local topography: these limits may typically both be ~100 MPa (Tables 1 and 2).

Some normal-fault-bounded structures are much wider than the examples considered in this study. For example, the Jeanne d'Arc basin has width H (of syn-rift sediments) ~110 km, and can be modelled flexurally with effective elastic thickness 10 km (Kusznir *et al.* 1991), comparable to the seismogenic thickness of the brittle layer. A profile across this basin (from fig. 13d of Kusznir *et al.* 1991) has T ~14 km, making r ~430 km. With a neutral fibre at 5 km depth, maximum bending strain for flexure would be $\leqslant 0.01$ and bending stress $\leqslant 1$ GPa for Young's modulus 75 GPa. Although near the limits, these are feasible values for flexure. It is thus reasonable that this basin developed by this process, retaining long-term elastic moduli similar to typical short-term values. Kusznir *et al.* (1991) suggested that most local extension was taken up by a single normal fault, which developed ~14 km of heave with final dip ~55°. Its throw would thus have been ~20 km, ~14 km of which contributed to syn-rift hanging-wall subsidence and the remainder created a ~6 km high footwall escarpment that subsequently eroded. The vertical stress associated with this ~20 km of relief would have been $\leqslant 0.6$ GPa, comparable to the estimated bending stress. Structures on this scale may thus develop entirely by flexure, even though narrower examples with sharper curvature may develop by vertical shear instead.

It is important to emphasize that the derivation of the expected general form of profiles of tilting (equation 8) did not address equilibrium considerations, either locally or for each fault zone as a whole. Treating the surroundings on each side of a fault as a whole, vertical equilibrium for the static situation after extension and tilting have ceased and shear stress has relaxed involves a balance between buoyancy forces and frictional forces acting on the fault. For the hanging-wall as a whole, the upward buoyancy force F_b (per unit along-strike length) is balanced by the downward component of friction

on the fault. From equation (5), with $H = 10$ km and $r = 30$ km, F_b is ~180 GN m^{-1}. With fault dip 45° and vertical extent 10 km, the average frictional stress on the fault needs to be only ~10 MPa. This is much smaller than likely limiting values (e.g. Turcotte & Schubert 1982, pp. 351–357), and can thus be readily supported. Full treatment of the equilibrium of each point within the brittle layer is difficult, and is beyond the scope of this study.

CONCLUSIONS

A generalized equation for profiles of tilting near normal faults, which gives a reasonable match to observations, is derived using calculus of variations. This equation is used to investigate whether flexure or distributed vertical simple shear causes these profiles for cumulative tilting across typical structures that are ≤15 km wide. The same general equation can also match coseismic elevation change. For long-term deformation, vertical shear typically requires less strain energy and lower maximum stress, and is thus favoured on both criteria. The ~100 MPa maximum shear stress is comparable to the maximum vertical and horizontal stresses. This long-term deformation can be regarded as a combination of repeated coseismic slip plus interseismic relaxation of bending stress that converts the deformation to vertical shear. The observation that the widths of the long-term and coseismic deformation around normal faults are typically the same, which has previously been interpreted following flexural modelling as evidence that the long-term 'effective elastic thickness' of the upper crust is low, is explicable instead if this relaxation mechanism only operates in localities that are displaced coseismically. This is reasonable if the relaxation is by a process, such as pressure solution creep, that is driven by stress caused by the coseismic flexure.

Acknowledgements—Supported in part by Natural Environment Research Council Grant GR3/6967. I thank Nick Kusznir for helpful discussions, and Roger Buck and Ross Stein for thoughtful reviews that prompted numerous improvements to the manuscript.

REFERENCES

Anders, M. H., Geissman, J. W., Piety, L. M. & Sullivan, J. T. 1989. Parabolic distribution of circumeastern Snake River Plain seismicity and latest Quaternary faulting: Migratory pattern and association with the Yellowstone hotspot. *J. geophys. Res.* **94**, 1589–1621.

Anderson, H., Smith, E. & Robinson, R. 1990. Normal faulting in a back arc basin: Seismological characteristics of the March 2, 1987, Edgecumbe, New Zealand, earthquake. *J. geophys. Res.* **95**, 4709–4723.

Axen, G. J. & Wernicke, B. P. 1989. Reply to comment by Carpenter, D. G., Carpenter, J. A., Bradley, M. D., Franz, U. A. & Reber, S. J. on "On the role of isostasy in the evolution of normal fault systems" by Wernicke, B. P. & Axen, G. J. *Geology* **17**, 775–776.

Ayres, F., Jr. 1972. *Theory and Problems of Differential and Integral Calculus* (2nd edn). McGraw-Hill, New York.

Barrientos, S. E., Stein, R. S. & Ward, S. N. 1987. Comparison of the 1959 Hebgen Lake, Montana, and the 1983 Borah Peak, Idaho, earthquakes from geodetic observations. *Bull. seism. Soc. Am.* **77**, 784–808.

Beanland, S., Blick, G. H. & Darby, D. J. 1990. Normal faulting in a back arc basin: Geological and geodetic characteristics of the 1987 Edgecumbe earthquake, New Zealand. *J. geophys. Res.* **95**, 4693–4707.

Buck, W. R. 1988. Flexural rotation of normal faults. *Tectonics* **7**, 959–973.

Dixon, J. S. 1978. Regional structural synthesis, Wyoming salient of western overthrust belt. *Bull. Am. Ass. Petrol. Geol.* **66**, 1560–1580.

Doser, D. I. 1985. Source parameters and faulting processes of the 1959 Hebgen Lake, Montana, earthquake sequence. *J. geophys. Res.* **90**, 4537–4566.

Doser, D. I. 1986. Earthquake processes in the Rainbow Mountain–Fairview Peak–Dixie Valley, Nevada, region 1954–1959. *J. geophys. Res.* **91**, 12,572–12,586.

Doser, D. I. & Smith, R. B. 1985. Source parameters of the October 28, 1983, Borah Peak earthquake from body wave analysis. *Bull. seism. Soc. Am.* **75**, 1041–1051.

Doser, D. I. & Smith, R. B. 1989. An assessment of source parameters of earthquakes in the cordillera of the western United States. *Bull. seism. Soc. Am.* **79**, 1383–1409.

Gilbert, C. M. & Reynolds, M. W. 1973. Character and chronology of basin development, western margin of the Basin and Range province. *Bull. geol. Soc. Am.* **84**, 2489–2510.

Jackson, J. A. 1987. Active normal faulting and crustal extension. In: *Continental Extensional Tectonics* (edited by Coward, M. P., Dewey, J. F. & Hancock, P. L.). *Spec. Publs geol. Soc. Lond.* **28**, 3–17.

Jackson, J. A., Gagnepain, J., Houseman, G., King, G., Papadimitriou, P., Soufleris, C. & Virieux, J. 1982. Seismicity, normal faulting, and the geomorphological development of the Gulf of Corinth (Greece): the Corinth earthquakes of February and March 1981. *Earth Planet. Sci. Lett.* **57**, 377–397.

Jackson, J. A. & McKenzie, D. P. 1983. The geometrical evolution of normal fault systems. *J. Struct. Geol.* **5**, 471–482.

Jackson, J. A. & White, N. J. 1989. Normal faulting in the upper continental crust: observations from regions of active extension. *J. Struct. Geol.* **11**, 15–36.

King, G. C. P. & Ellis, M. 1990. The origin of large local uplift in extensional regions. *Nature* **348**, 689–693.

King, G. C. P., Stein, R. S. & Rundle, J. B. 1988. The growth of geological structures by repeated earthquakes: 1. conceptual framework. *J. geophys. Res.* **93**, 13,307–13,318.

Koseluk, R. A. & Bishke, R. E. 1981. An elastic rebound model for normal fault earthquakes. *J. geophys. Res.* **86**, 1081–1090.

Kusznir, N. J. & Egan, S. S. 1990. Simple-shear and pure-shear models of extensional sedimentary basin formation: Application to the Jeanne d'Arc basin, Grand Banks of Newfoundland. In: *Extensional Tectonics and Stratigraphy of the North Atlantic Margins* (edited by Tankard, A. J. & Balkwill, H. R.). *Mem. Am. Ass. Petrol. Geol.* **46**, 305–322.

Kusznir, N. J., Marsden, G. & Egan, S. 1991. A flexural-cantilever simple-shear/pure-shear model of continental extension: applications to the Jeanne d'Arc basin, Grand Banks, and Viking graben, North Sea. In: *The Geometry of Normal Faults* (edited by Roberts, A., Yielding, G. & Freeman, B.). *Spec. Publs geol. Soc. Lond.* **56**, 41–60.

Mabey, D. R. 1985. Regional gravity and magnetic anomalies in the Borah Peak region of Idaho. In: *Proc. Workshop 28 on the Borah Peak, Idaho, earthquake. U.S. geol. Surv. Open-file Rep.* **85-290A**, 680–686.

Mansinha, L. & Smylie, D. E. 1971. The displacement fields of inclined faults. *Bull. seism. Soc. Am.* **61**, 1433–1440.

Mariolakos, I. & Stiros, S. C. 1987. Quaternary deformation of the Isthmus and Gulf of Corinthos (Greece). *Geology* **15**, 225–228.

Marsden, G., Yielding, G., Roberts, A. M. & Kusznir, N. J. 1990. Application of a flexural cantilever simple-shear/pure-shear model of continental lithosphere extension to the formation of the northern North Sea basin. In: *Tectonic Evolution of the North Sea Rift* (edited by Blundell, D. J.). Oxford University Press, Oxford, 236–257.

Pantosti, D. & Valensise, G. 1990. Faulting mechanism and complexity of the 23 November 1980 Campania–Lucania earthquake inferred from surface observations. *J. geophys. Res.* **95**, 15,319–15,341.

Ranalli, G. 1987. *Rheology of the Earth: Deformation and Flow Processes in Geophysics and Geodynamics*. Allen & Unwin, London.
Reil, O. E. 1957. Damage to Nevada highways. *Bull. seism. Soc. Am.* **47**, 349–352.
Reilinger, R. E. 1986. Evidence for postseismic viscoelastic relaxation following the 1959 **M** = 7.5 Hebgen Lake earthquake. *J. geophys. Res.* **91**, 9488–9494.
Richins, W. D., Pechmann, J. C., Smith, R. B., Langer, C. J., Goter, S. K., Zollweg, J. E. & King, J. J. 1987. The 1983 Borah Peak, Idaho, earthquake and its aftershocks. *Bull. seism. Soc. Am.* **77**, 694–723.
Riley, K. F. 1974. *Mathematical Methods for the Physical Sciences*. Cambridge University Press, Cambridge.
Roberts, A. M. & Yielding, G. 1991. Deformation around basin-margin faults in the North Sea/mid-Norway rift. In: *The Geometry of Normal Faults* (edited by Roberts, A., Yielding, G. & Freeman, B.). *Spec. Publs geol. Soc. Lond.* **56**, 61–78.
Romney, C. 1957. Seismic waves from the Dixie Valley–Fairview Peak earthquakes. *Bull. seism. Soc. Am.* **47**, 301–319.
Savage, J. C. & Hastie, L. M. 1966. Surface deformation associated with dip-slip faulting. *J. geophys. Res.* **71**, 4897–4904.
Savage, J. C. & Hastie, L. M. 1969. A dislocation model for the Fairview Peak, Nevada, earthquake. *Bull. seism. Soc. Am.* **59**, 1937–1948.
Schwartz, D. P. & Coppersmith, K. J. 1984. Fault behavior and characteristic earthquakes: examples from the Wasatch and San Andreas fault zones. *J. geophys. Res.* **89**, 5681–5698.
Slemmons, D. B. 1957. Geological effects of the Dixie Valley–Fairview Peak, Nevada, earthquakes. *Bull. seis. Soc. Am.* **47**, 353–375.
Stein, R. S. & Barrientos, S. E. 1985. High-angle normal faulting in the Intermountain seismic belt: Geodetic investigation of the 1983 Borah Peak, Idaho, earthquake. *J. geophys. Res.* **90**, 11,355–11,366.
Stein, R. S., King, G. C. P. & Rundle, J. B. 1988. The growth of geological structures by repeated earthquakes: 2. field examples of continental dip-slip faults. *J. geophys. Res.* **93**, 13,319–13,331.
Turcotte, D. L. & Schubert, G. 1982. *Geodynamics: Applications of Continuum Physics to Geological Problems*. Wiley, New York.
Verrall, P. 1981. Structural interpretation with application to North Sea problems. Course notes No. 3, Joint Association for Petroleum Exploration Courses (U.K.).
Ward, S. N. 1986. A note on the surface volume change of shallow earthquakes. *Geophys. J. R. astr. Soc.* **85**, 461–466.
Weissel, J. K. & Karner, G. D. 1989. Flexural uplift of rift flanks due to mechanical unloading of the lithosphere during extension. *J. geophys. Res.* **94**, 13,919–13,950.
Wernicke, B. 1985. Uniform sense normal simple shear of the continental lithosphere. *Can. J. Earth Sci.* **22**, 108–125.
Wernicke, B. & Axen, G. J. 1988. On the role of isostasy in the evolution of normal fault systems. *Geology* **16**, 848–851.
Westaway, R. 1987. Comment on "The southern Italy earthquake of 23 November 1980" by Crosson, R. S., Martini, M., Scarpa, R. & Key, S. C. *Bull. seism. Soc. Am.* **77**, 1071–1074.
Westaway, R. 1989. Deformation of the NE Basin and Range province: the response of the lithosphere to the Yellowstone plume. *Geophys. J. Int.* **99**, 33–62 (with 1991 correction: **104**, 647–659).
Westaway, R. 1990. Reply to comment by Anders, M. H., Geissman, J. W. & Sleep, N. H., on "Northeastern Basin and Range province active tectonics: an alternative view" by R. Westaway. *Geology* **18**, 915–917.
Westaway, R. 1991. Continental extension on sets of parallel faults: observational evidence and theoretical models. In: *The Geometry of Normal Faults* (edited by Roberts, A., Yielding, G. & Freeman, B.). *Spec. Publs geol. Soc. Lond.* **56**, 143–169.
Westaway, R., Gawthorpe, R. & Tozzi, M. 1989. Seismological and field observations of the 1984 Lazio–Abruzzo earthquakes: Implications for the active tectonics of Italy. *Geophys. J.* **98**, 489–514.
Westaway, R. & Jackson, J. A. 1987. The earthquake of 1980 November 23 in Campania–Basilicata (southern Italy). *Geophys. J. R. astr. Soc.* **90**, 375–443.
Westaway, R. & Kusznir, N. J. 1990. Neogene evolution of the Aegean region. *Eos* **71**, 1634.
Westaway, R. & Kusznir, N. J. In press. Fault and bed 'rotation' during continental extension: block rotation or vertical shear? *J. Struct. Geol.*
White, N. J., Jackson, J. A. & McKenzie, D. P. 1986. The relationship between the geometry of normal faults and that of the sedimentary layers in their hanging walls. *J. Struct. Geol.* **8**, 897–909.
Whitten, C. A. 1957. Geodetic investigations in the Dixie Valley area. *Bull. seism. Soc. Am.* **47**, 321–325.

APPENDIX A

DERIVATION OF PROFILES OF TILTING

One can find a stationary value (which in this case is a minimum) for any integral of the form $\int f(w, w')dx$ using the first integral of Euler's equation (see, e.g. Riley 1974, pp. 332–346). For such an integral to be stationary,

$$f - w' \frac{\partial f}{\partial w'} = B, \tag{A1}$$

where B is a constant.

The condition that minimizes the integral in equation (7) in the main text is thus

$$jw + (1 + w'^2)^{1/2} - w'^2(1 + w'^2)^{1/2} = B \tag{A2}$$

$$dx = \frac{B - jw}{(1 - (B - jw)^2)^{1/2}} dw. \tag{A3}$$

This has the solution

$$x + c = \frac{(1 - (B - jw)^2)^{1/2}}{j} \tag{A4}$$

or

$$j^2(x + c)^2 = 1 - (B - jw)^2, \tag{A5}$$

where c is a constant of integration. Differentiating equation (A5) gives

$$2j^2(x + c)^2 = 2j(B - jw)w'. \tag{A6}$$

If $x = 0$ where $w = 0$, then

$$j^2c^2 = 1 - B^2 \tag{A7}$$

and if $x = 0$ where $w' = 0$, then:

$$jc^2 = 0 \tag{A8}$$

which requires $c = 0$ except for a trivial solution. This requires $B \pm 1$. With $B = 1$,

$$1 - j^2x^2 = (1 - jw)^2. \tag{A9}$$

The solution with $B = -1$ has the same form but with a change of sign for j.

With $B = 1$, the boundary condition that $w(H) = T$ (T being the deflection at the fault—see Fig. 2) gives $j = 2T/(T^2 + H^2)$ or $j = 0$, the latter also being a trivial solution. The former gives $j \sim 2T/H^2$ since $H \gg T$. If r is defined as $1/j$, then, typically, $r \gg H$ since $H \gg T$, and

$$r = (H^2 + T^2)/2T \sim H^2/2T. \tag{A10}$$

Equation (A4) can then be rearranged such that

$$w = r(1 - (1 - x^2/r^2)^{1/2}). \tag{A11}$$

Thus

$$w' = (x/r)(1 - x^2/r^2)^{-1/2} \tag{A12}$$

$$w'' = (1/r)(1 - x^2/r^2)^{-3/2} \tag{A13}$$

and

$$w''' = (3x/r^3)(1 - x^2/r^2)^{-5/2}. \tag{A14}$$

With $w \ll r$ equation (A9) can be well approximated as

$$1 - x^2/r^2 = 1 - 2w/r + O(w^2/r^2), \tag{A15}$$

where $O(w^2/r^2)$ means terms of the order of w^2/r^2, which are neglected. This gives:

$$w = x^2/2r \tag{A16}$$

$$w' = x/r \tag{A17}$$

and

$$w'' = 1/r. \tag{A18}$$

To first order:

$$w''' = 3x/r^3. \tag{A19}$$

This approximate solution is thus a parabola with radius of curvature $r \sim H^2/2T$.

APPENDIX B

ELASTIC STRAIN ENERGY

This Appendix estimates the elastic strain energy in part of the brittle layer near any normal fault that is deflected to accommodate slip on the normal fault, under the alternative assumptions of distributed vertical simple shear and flexure.

Strain energy assuming distributed vertical simple shear

Under distributed vertical simple shear, at each locality shear strain $\varepsilon_{xz} = (1/2)w'$ and shear stress $\sigma_{xz} = \mu w'$. The resulting strain energy density q_s equals $(\mu/4)w'^2$. Shear stress thus increases towards each fault as w' increases, and if the shear strain is uniform at the fault and decreases uniformly with distance from it at each depth, it will be uniform at all depths within the brittle layer at each distance from the fault. Total elastic strain energy (per unit along-strike length) for these stress and strain tensor elements is thus

$$Q_s = \int q_s(x, z)\, dz\, dx, \tag{B1}$$

where z spans 0–Z (the brittle layer thickness) and x spans 0–H (assuming the same width of tilting at all depths; Fig. 2b). With w' given by equation (A12), then:

$$Q_s = \frac{\mu}{4}\int_{z=0}^{Z} dz \int_{x=0}^{H} \frac{x^2}{r^2 - x^2}\, dx. \tag{B2}$$

Hence,

$$Q_s = \frac{\mu Z}{8}\int_{x=0}^{H} \frac{x}{r-x} - \frac{x}{r+x}\, dx \tag{B3}$$

$$Q_s = \frac{\mu Z}{8}\left[r \ln \frac{r+H}{r-H} - 2H\right]. \tag{B4}$$

With $r \sim 3H$,

$$Q_s = \frac{\mu Z r}{8}[\ln 2 - 2/3] \tag{B5}$$

$$Q_s = 0.003310 \mu Z r \quad \text{(exact)}. \tag{B6}$$

Strain energy for distributed vertical simple shear is thus proportional to the thickness of the brittle layer and its radius of curvature.

An approximation to equation (B1) can be obtained for $H/r \ll 1$, when $w' \sim x/r$:

$$Q_s = \frac{\mu}{4r^2}\int_{z=0}^{Z} dz \int_{x=0}^{H} x^2\, dx \tag{B7}$$

$$Q_s = \frac{\mu Z H^3}{12 r^2} \quad \text{(approx.)}. \tag{B8}$$

This does not look like equation (B4). However, with $H = r/3$ it gives

$$Q_s = 0.003086 \mu Z r \quad \text{(approx.)} \tag{B9}$$

which differs from equation (B6) by only ~12%, the exact estimate being the larger. With $r \geq 3H$, equation (B8) is thus a good approximation to equation (B5).

The total strain energy for distributed simple shear will be double each of the above estimates, taking account of the contribution from σ_{zx} and ε_{zx}, which equal σ_{xz} and ε_{xz} since the stress and strain tensors are symmetric.

Strain energy assuming flexure

For flexure, bending strain ε_{xx} and stress σ_{xx} are given by equations (1) and (2). Both are proportional to w'' and to distance above and below the neutral fibre $(z - z_0)$. In the absence of brittle failure, $z_0 = Z/2$, and the largest bending stress is expected at the top and base of the brittle layer. With w'' only a weak function of x in equation (A13), bending strain and stress at constant z will vary little as one moves away from the fault. Their contribution to strain energy density is thus:

$$q_f = \frac{E(z - z_0)^2 w''^2}{2(1 - \nu^2)} \tag{B10}$$

and resulting elastic strain energy is thus

$$Q_f = \frac{E r^4}{2(1-\nu^2)}\int_{z=0}^{z=Z} (z - z_0)^2\, dz \int_{x=0}^{x=H} \frac{1}{(r^2 - x^2)^3}\, dx \tag{B11}$$

$$Q_f = \frac{EZ^3}{24(1-\nu^2)r^2}\int_{x=0}^{x=H} \frac{1}{(1 - x^2/r^2)^3}\, dx. \tag{B12}$$

This may be written as:

$$Q_f = \frac{EZ^3}{24(1-\nu^2)r^2} J, \tag{B13}$$

where

$$J = \int_{x=0}^{x=H} \frac{1}{(1 - x^2/r^2)^3}\, dx. \tag{B14}$$

To evaluate this, substitute $x = r \cos(u)$ to give

$$J = r\int_{u=\pi/2}^{u=\text{arc cos}\,(H/r)} \text{cosec}^5(u)\, du. \tag{B15}$$

This appears worse than (B14), but, fortunately, has been solved (see e.g. Ayers 1972, p. 146, equation 27.59): the indefinite integral I of $\text{cosec}^5(u)$ is

$$I = -\frac{1}{4}\text{cosec}^3(u)\cot(u) - \frac{3}{8}\text{cosec}(u)\cot(u) + \frac{3}{8}(\ln|\text{cosec}(u) - \cot(u)|) + c, \tag{B16}$$

with c another constant of integration. With the limits of integration in equation (B15), noting that $\text{cosec}(\pi/2) = 1$ and $\cot(\pi/2) = 0$ and that if $\cos(u) = H/r$ then $\text{cosec}(u) = (1 - H^2/r^2)^{-1/2}$ and $\cot(u) = (H/r)(1 - H^2/r^2)^{-1/2}$, from equation (B16):

$$J = \frac{1}{8}\left[\frac{2H}{(1 - H^2/r^2)^2} + \frac{3H}{(1 - H^2/r^2)} - 3r \ln\left(\frac{1 - H/r}{(1 - H^2/r^2)^{1/2}}\right)\right]. \tag{B17}$$

Hence, the resulting elastic strain energy is

$$Q_f = \frac{1}{192}\left[\frac{2H}{(1 - H^2/r^2)^2} + \frac{3H}{(1 - H^2/r^2)} - 3r \ln\left(\frac{1 - H/r}{(1 - H^2/r^2)^{1/2}}\right)\right]\frac{EZ^3}{(1-\nu^2)r^2} \quad \text{(exact)}. \tag{B18}$$

As a check, an approximate solution to equation (B11) can be derived by substituting $w'' = 1/r$, the limit when $H \ll r$, to obtain:

$$Q_f = \frac{E}{2(1-\nu^2)}\int_{z=0}^{z=Z} (z - z_0)^2 \int_{x=0}^{x=H} \frac{1}{r^2}\, dx \tag{B19}$$

$$Q_f = \frac{EHZ^3}{24(1-\nu^2)r^2} \quad \text{(approx.)}. \tag{B20}$$

Bearing in mind that $\ln(1 - x) \cong -x$ when $x \ll 1$, equation (B17) simplifies to $J = H$ when $H/r \ll 1$. Hence, the limit of equation (B18) with $H/r \ll 1$ is the same as equation (B20). For $H = r/3$ equation (B18) gives

$$Q_f = 0.01567 \frac{EZ^3}{(1-\nu^2)r} \quad \text{(exact)} \tag{B21}$$

and equation (B20) gives

$$Q_f = 0.01399 \frac{EZ^3}{(1-\nu^2)r} \quad \text{(approx.)}, \tag{B22}$$

which differ by only ~11%, the exact estimate again being the larger. For flexure, elastic strain energy associated with the σ_{xx} and ε_{xx} terms is thus expected to be proportional to the width of tilting and the cube of brittle layer thickness, and inversely proportional to the square of its radius of curvature.

The σ_{zz} stress tensor element is assumed zero to derive equation (2). However, the σ_{xz} and σ_{zx} elements will be non-zero, and will add to the strain energy. To estimate their contribution, consider the bending moment M for flexure:

$$M(x) = -\frac{EZ^3 w''(x)}{12(1-\nu^2)}. \tag{B23}$$

The vertical shear force on each element of width dx is $F = dM/dx$, where:

$$F = \int_{z=0}^{Z} \sigma_{xz}\, dz. \tag{B24}$$

Hence

$$F = -\frac{EZ^3 w'''(x)}{12(1-\nu^2)} \tag{B25}$$

and, since F is not a function of z,

$$\sigma_{xz} = \frac{EZ^2 w'''(x)}{12(1-\nu^2)}. \tag{B26}$$

The corresponding shear strain is $\varepsilon_{xz} = \sigma_{xz}/(2\mu)$, and the strain energy density is thus:

$$q_t = \frac{E^2 Z^4 w'''(x)^2}{576\mu(1-\nu^2)^2} \tag{B27}$$

or, since $E = 2\mu(1+\nu)$,

$$q_t = \frac{EZ^4 w'''(x)^2}{288(1-\nu^2)(1-\nu)}. \tag{B28}$$

This can be solved approximately using w''' from equation (A19):

$$Q_t = \frac{3EH^3 Z^5}{288(1-\nu^2)(1-\nu)r^6} \quad \text{(approx.)}. \tag{B29}$$

For $H = r/3$ this gives

$$Q_t = \frac{EZ^5}{7776(1-\nu^2)(1-\nu)r^3} \quad \text{(approx.)}. \tag{B30}$$

Even when this is doubled to account for the other off-diagonal elements of the stress and strain tensors, its contribution will be very small for $Z \leqslant r$.